PCCP

PAPER

View Article Online
View Journal | View Issue

Cite this: *Phys. Chem. Chem. Phys.*, 2016, **18**, 21102

Planar *vs.* three-dimensional X_6^{2-}, $X_2Y_4^{2-}$, and $X_3Y_3^{2-}$ (X, Y = B, Al, Ga) metal clusters: an analysis of their relative energies through the turn-upside-down approach†‡

Ouissam El Bakouri,[a] Miquel Solà*[a] and Jordi Poater*[bcd]

Received 18th February 2016, Accepted 11th March 2016

DOI: 10.1039/c6cp01109h

www.rsc.org/pccp

Despite the fact that B and Al belong to the same group 13 elements, the B_6^{2-} cluster prefers the planar D_{2h} geometry, whereas Al_6^{2-} favours the O_h structure. In this work, we analyse the origin of the relative stability of D_{2h} and O_h forms in these clusters by means of energy decomposition analysis based on the turn-upside-down approach. Our results show that what causes the different trends observed is the orbital interaction term, which combined with the electrostatic component do (Al_6^{2-} and Ga_6^{2-}) or do not (B_6^{2-}) compensate the higher Pauli repulsion of the O_h form. Analysing the orbital interaction term in more detail, we find that the preference of B_6^{2-} for the planar D_{2h} form has to be attributed to two particular molecular orbital interactions. Our results are in line with a dominant delocalisation force in Al clusters and the preference for more localised bonding in B metal clusters. For mixed clusters, we have found that those with more than two B atoms prefer the planar structure for the same reasons as for B_6^{2-}.

Introduction

The electronic distribution of nanosized molecular clusters can be very different from that of the bulk state.[1] In fact, metals can exhibit isolating behaviour when reduced to small particles. Since the electronic properties of nanoparticles are quite different from those of the bulk, molecular clusters are expected to have a variety of electronic applications, such as single-electron transistors, diodes, and quantum dots.[2–4] The properties of clusters are profoundly affected by the type of bonding they have. For some of these clusters one can expect an intermediate situation between covalent and metallic bonding. As modern technologies evolve towards the nanoscale, it becomes more important to have a more precise understanding of the bonding in these species to better tune their properties.

Among clusters, those made by group 13 atoms are particularly important.[5] Both B and Al belong to the same group 13, and thus present a similar electronic structure, [He]$2s^22p^1$ and [Ne]$3s^23p^1$, respectively. However, when they form small clusters, B clusters adopt a planar conformation as the equilibrium structure;[6–9] whereas Al clusters present a three-dimensional (3D) closed shape.[10–13] The most relevant examples are B_6^{2-} and Al_6^{2-} clusters, which were obtained experimentally as lithium salts in the form of LiB_6^- and $LiAl_6^-$.[14–16] B_6^{2-} adopts a planar D_{2h} geometry in its low-lying singlet state, whereas the Al_6^{2-} cluster is octahedral. Both shapes of the metal clusters are kept when lithium salts are formed.

The chemical bonding of B_6^{2-} and Al_6^{2-} has been widely analysed in previous studies.[14,17,18] In particular, Alexandrova *et al.*[18] highlighted the fact that B_6^{2-} is able to 2s–2p hybridize and to form 2-center–2-electron (2c–2e) B–B covalent localised bonds. On the other hand, 3s–3p hybridisation in the Al_6^{2-} cluster is more difficult due to larger s–p energy separation, which hampers the formation of directional covalent Al–Al bonds.[19] In this case, bonding comes from the combination of radial and tangential p-orbitals that result in extensive delocalisation.[20] Indeed, the Al_6^{2-} cluster displays octahedral aromaticity,[14,21] whereas planar D_{2h} B_6^{2-} is considered σ- and π-antiaromatic.[17,18,22,23] Thus, as pointed out by Alexandrova *et al.*,[18,24–26] covalent and delocalised bonding shows opposite

[a] Institut de Química Computacional i Catàlisi (IQCC) and Departament de Química, Universitat de Girona, Campus Montilivi, 17071 Girona, Catalonia, Spain. E-mail: miquel.sola@udg.edu

[b] Departament de Química Inorgànica i Orgànica & Institut de Química Teòrica i Computacional (IQTCUB), Universitat de Barcelona, Martí i Franquès 1-11, 08028 Barcelona, Catalonia, Spain. E-mail: jordi.poater@gmail.com

[c] Department of Theoretical Chemistry and Amsterdam Center for Multiscale Modeling, Vrije Universiteit Amsterdam, De Boeleaan 1083, NL-1081HV Amsterdam, The Netherlands

[d] Institució Catalana de Recerca i Estudis Avançats (ICREA), Pg. Lluís Companys 23, 08010 Barcelona, Catalonia, Spain

† This work is dedicated to Prof. Evert Jan Baerends as a proof of our admiration for his brilliant contributions to chemistry and of our gratitude for helping us to understand chemistry better.

‡ Electronic supplementary information (ESI) available. See DOI: 10.1039/c6cp01109h

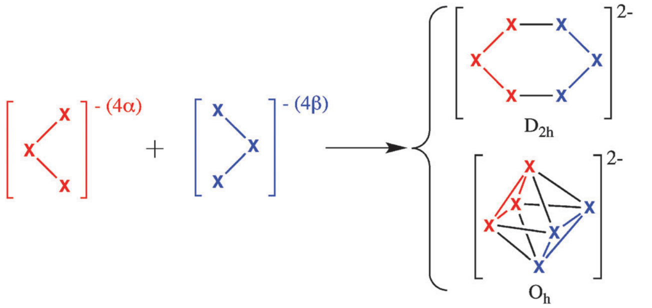

Scheme 1 D_{2h} and O_h structures of X_6^{2-} can be formed from C_{2v} X_3^- fragments.

effects in determining the molecular structure of many clusters. Huynh and Alexandrova analysed the whole series $B_nAl_{6-n}^{2-}$ (n = 0–6), from B_6^{2-} till Al_6^{2-} by substituting one B by Al each time, concluding that covalent bonding is a resilient effect that governs the cluster shape more than delocalisation does. Indeed, the planar structure of B_6^{2-} persists until n = 5, the reason being the strong tendency to form 2c–2e B–B bonds in case the cluster contains two or more B atoms.[18] Similar results were reported by Fowler and Ugalde in larger clusters of group 13. In particular, these authors found that B_{13}^+ prefers a planar conformation[27] in contrast to Al_{13}^-,[28] which adopts an icosahedral geometry. Interestingly, in *closo* boranes and substituted related species, like $B_6H_6^{2-}$ or $B_{12}I_{12}^{2-}$, the delocalised 3D structure is preferred. However, successive stripping of iodine in $B_{12}I_{12}^{2-}$ leads to a B_{12} planar structure with some localised 2c–2e B–B bonds.[29,30] Similarly, for $B_6H_n^-$ clusters, the clusters are planar for $n \leq 3$ and become tridimensional for $n \geq 4$.[31]

As can be seen in Scheme 1, both 2D D_{2h} planar and 3D O_h geometries for X_6^{2-} (X = B, Al) can be obtained joining the same two X_3^- cluster fragments.[14,17] Therefore, X_6^{2-} species in D_{2h} and O_h geometries are particularly suitable for an energy decomposition analysis (EDA)[32–35] based on the turn-upside-down approach.[36–39] In this approach, two different isomers are formed from the same fragments and the bonding energy is decomposed into different physically meaningful components using an EDA. Differences in the energy components explain the reasons for the higher stability of the most stable isomer. For instance, using this method we provided an explanation of why the cubic isomer of T_d geometry is more stable than the ring structure with D_{4h} symmetry for $(MX)_4$ tetramers (X = H, F, Cl, Br, and I) if M is an alkalimetal and the other way round if M belongs to group 11 transition metals.[38] Therefore, the application of this type of analysis to B_6^{2-} and Al_6^{2-} clusters will disclose the factors that make the planar D_{2h} structure more stable for boron and the octahedral one for aluminium. As said before, boron clusters favour localised covalent bonds whereas aluminium clusters prefer a more delocalised bonding. With the present analysis, we aim to provide a more detailed picture of the reasons for the observed differences. The analysis will be first applied to the above referred B_6^{2-} and Al_6^{2-} clusters, and then further complemented with Ga_6^{2-}. Finally, $X_2Y_4^{2-}$ and $X_3Y_3^{2-}$ (X, Y = B, Al, Ga) mixed clusters in their distorted D_{2h} planar and 3D D_{4h} geometries will also be discussed.

Computational methods

All Density Functional Theory (DFT) calculations were performed using the Amsterdam Density Functional (ADF) program.[40] The molecular orbitals (MOs) were expanded in a large uncontracted set of Slater type orbitals (STOs) of triple-ζ quality for all atoms (TZ2P basis set). The 1s core electrons of boron, 1s–2p of aluminium, and 1s–3p of gallium were treated by the frozen core approximation. Energies and gradients were computed using the local density approximation (Slater exchange and VWN correlation) with non-local corrections for exchange (Becke88) and correlation (Lee–Yang–Parr 1988) included self-consistently (*i.e.* the BLYP functional). D3(BJ) dispersion corrections by Grimme were also included in the functional (*i.e.* BLYP-D3(BJ) functional).[41–44] Analytical Hessians were computed to confirm the nature of the located minima at the same level of theory.

Relative energies between the planar and 3D species were also calculated using the Gaussian 09 program[45] at the coupled cluster level[46] with single and double excitation (CCSD)[47] and with triple excitation treated perturbatively (CCSD(T))[48] using Dunning's correlation consistent augmented triple-ζ (aug-cc-pVTZ)[49,50] at optimised BLYP-D3(BJ)/TZ2P molecular geometries.

The bonding energy corresponding to the formation of X_6^{2-} for both D_{2h} and O_h symmetries from two anionic quintet tetraradicals, fragment 1 (αααα) + fragment 2 (ββββ) (see Scheme 1), is made up of two major components (eqn (1)):

$$\Delta E = \Delta E_{\mathrm{dist}} + \Delta E_{\mathrm{int}} \qquad (1)$$

In this formula, the distortion energy ΔE_{dist} is the amount of energy required to deform the separated tetraradical fragments in their quintet state from their equilibrium structure to the geometry that they acquire in the metal cluster. The interaction energy ΔE_{int} corresponds to the actual energy change when the prepared fragments are combined to form the overall molecule. It is analysed in the framework of the Kohn–Sham MO model using a Morokuma-type decomposition[32–35] of the bonding energy into electrostatic interaction, exchange (or Pauli) repulsion, orbital interactions, and dispersion forces (eqn (2)).

$$\Delta E_{\mathrm{int}} = \Delta V_{\mathrm{elstat}} + \Delta E_{\mathrm{Pauli}} + \Delta E_{\mathrm{oi}} + \Delta E_{\mathrm{disp}} \qquad (2)$$

The term $\Delta V_{\mathrm{elstat}}$ corresponds to the classical electrostatic interaction between the unperturbed charge distributions of the prepared (*i.e.* deformed) fragments and is usually attractive. The Pauli repulsion $\Delta E_{\mathrm{Pauli}}$ comprises the destabilizing interactions between occupied MOs. It arises as the energy change associated with going from the superposition of the unperturbed electron densities of the two fragments to the wavefunction $\Psi^0 = NA\,[\Psi^{4\alpha}_{\mathrm{fragment1}}\cdot\Psi^{4\beta}_{\mathrm{fragment2}}]$, which properly obeys the Pauli principle through explicit antisymmetrisation (A operator) and renormalisation (N constant) of the product of fragment wavefunctions. It comprises four-electron destabilizing interactions between occupied MOs and is responsible for steric repulsion. The orbital interaction ΔE_{oi} is the change in energy from Ψ^0 to the final, fully converged wavefunction Ψ_{SCF} of the system. The orbital interactions account for charge transfer (*i.e.*, donor–acceptor interactions between occupied orbitals on one fragment with unoccupied orbitals of the other, including the HOMO–LUMO interactions) and polarization (empty – occupied orbital mixing on one fragment due to the presence of another fragment). Finally, the ΔE_{disp} term takes into account the interactions which are due to dispersion forces.

In bond-energy decomposition,[51–53] open-shell fragments were treated with spin-unrestricted formalism but, for technical reasons, spin-polarisation was not included. This error causes the studied bond to become in the order of a few kcal mol^{-1} too strong. To facilitate a straightforward comparison, the EDA results were scaled to match exactly the regular bond energies (the correction factor is consistently in the range 0.97–0.98 in all model systems and does therefore not affect trends). A similar scheme based on the same EDA approach was used by Frenking and coworkers[54,55] and by some of us[36,37,56] to estimate the strength of π-cyclic conjugation in typical (anti)-aromatic organic compounds and in metallabenzenes and metallacyclopentadienes.

Let us mention here that, as already mentioned in the introduction, some of the analysed metal clusters exist experimentally as lithium salts.[14–16] On the other hand, these dianionic systems are unstable against the ejection of an electron. However, their molecular and electronic structure is very similar to that of their corresponding lithium salts, which justifies the analysis of the chemical bonding of these doubly charged systems, as it is not affected by the presence of a lithium cation.

Finally, the metalloaromaticity[57] of these clusters was evaluated at the BLYP/aug-cc-pVDZ level of theory with the optimized BLYP-D3(BJ)/TZ2P geometries by means of multicentre electron sharing indices (MCIs).[58–60] MCIs provide a measure of electron sharing among the atoms considered,[59] in the present case the six atoms that form each of the clusters studied. MCI values have been calculated using the ESI-3D program.[61,62]

Results and discussion

We first focus on the homoatomic X_6^{2-} metal clusters with X = B, Al, and Ga. The optimized O_h and D_{2h} geometries at the BLYP-D3(BJ)/TZ2P level are depicted in Fig. 1 with the main bond lengths and angles. As expected, B–B bond lengths (1.536–1.768 Å) are much shorter than those for Al–Al (2.574–2.912 Å) and Ga–Ga (2.526–2.898 Å). The similar Al–Al and Ga–Ga distances in X_6^{2-} metal clusters (X = Al, Ga) are not unexpected given the similar van der Waals radii of these two elements.[63] In addition, the X–X bond length connecting the two equivalent X_3^- fragments in O_h clusters is longer than in the D_{2h} systems.

Table 1 encloses the energy differences between O_h and D_{2h} clusters. For B_6^{2-} D_{2h} symmetry is more stable than O_h by 67.5 kcal mol^{-1}, the latter not being a minimum.[18] Meanwhile the opposite trend is obtained in the other two metal clusters, for which O_h is lower in energy by 15.8 (Al_6^{2-}) and 9.3 kcal mol^{-1} (Ga_6^{2-}) than D_{2h} structures. These trends are confirmed by higher level CCSD(T)/aug-cc-pVTZ single point energy calculations at the same BLYP-D3(BJ)/TZ2P geometries (values also enclosed in

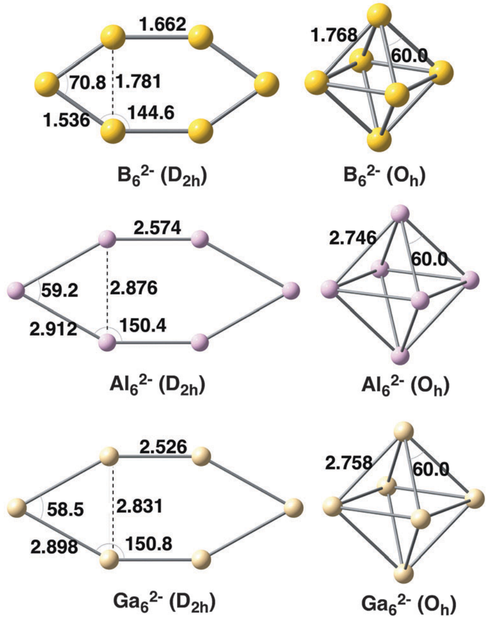

Fig. 1 Geometries of X_6^{2-} metal clusters analysed with D_{2h} and O_h symmetries. Distances in Å and angles in degrees.

Table 1 Relative energies of clusters between O_h and D_{2h} symmetries (in kcal mol^{-1}), and the aromatic MCI criterion

		BLYP-D3(BJ)/TZ2P[a]		CCSD(T)/aug-cc-pVTZ[b]		MCI[c]	
Clusters		O_h	D_{2h}	O_h	D_{2h}	O_h	D_{2h}
X_6^{2-}	B_6^{2-}	67.5[e]	0.0[d]	38.7	0.0	0.062	−0.052
	Al_6^{2-}	0.0[d]	15.8[e]	0.0	44.8	0.077	0.068
	Ga_6^{2-}	0.0[f]	9.3[f]	0.0	46.6	0.083	0.071

		BLYP-D3(BJ)/TZ2P[a]		CCSD(T)/aug-cc-pVTZ[b]		MCI[c]	
Clusters		D_{4h}	D_{2h}	D_{4h}	D_{2h}	D_{4h}	D_{2h}
$X_2Y_4^{2-}$	$B_2Al_4^{2-}$	0.0[g]	15.9[g]	0.0	34.0	0.032	0.001
	$Al_2B_4^{2-}$	66.9[h]	0.0[g]	48.7	0.0	0.032	0.023
	$Al_2Ga_4^{2-}$	0.0[d]	13.0[h]	0.0	43.3	0.077	0.068
	$Ga_2B_4^{2-}$	79.4[g]	0.0[g]	47.1	0.0	0.047	0.042
	$Ga_2Al_4^{2-}$	0.0[d]	14.8[g]	0.0	48.2	0.074	0.072

		BLYP-D3(BJ)/TZ2P[a]		CCSD(T)/aug-cc-pVTZ[b]		MCI[c]	
Clusters		D_{3h}	C_{3v}	D_{3h}	C_{3v}	D_{3h}	C_{3v}
$X_3Y_3^{2-}$	$Al_3Ga_3^{2-}$	0.0[d]	13.2[h]	0.0	45.3	0.078	0.068

[a] $B_2Ga_4^{2-}$ (D_{2h}) has not been obtained because optimization breaks the symmetry; whereas $B_3Al_3^{2-}$ and $B_3Ga_3^{2-}$ (O_h) have not been obtained because the strength of the B_3 unit causes the systems to be planar and to avoid a 3D geometry. [b] Single point energy calculations at BLYP-D3(BJ)/TZ2P geometries. [c] MCI calculated at the BLYP/aug-cc-pVDZ level of theory with the BLYP-D3(BJ)/TZ2P optimized geometries. [d] Local minima. [e] One imaginary frequency. [f] One small imaginary frequency due to numerical integration problems. [g] Two imaginary frequencies. [h] Three imaginary frequencies.

Table 1). The relative energies of B_6^{2-}, Al_6^{2-}, and Ga_6^{2-} between O_h and D_{2h} symmetries are now −38.7, +44.8 and +46.6 kcal mol^{-1}, respectively. CCSD(T) values systematically favour O_h as compared to D_{2h} structures by about 20–30 kcal mol^{-1}. However, the qualitative picture remains the same.

The aromaticity of these X_6^{2-} metal clusters was evaluated by means of the MCI electronic criterion. The six-membered MCIs are enclosed in Table 1. In all cases, the O_h system is more aromatic than the D_{2h} one, in agreement with the larger electronic delocalisation of the former, as discussed in the Introduction.[21] MCI values confirm the octahedral aromaticity[21] of O_h Al_6^{2-} and the antiaromatic character of D_{2h} B_6^{2-}.[17,18,22,23] Interestingly, MCI values point out the clear aromatic character of all 3D clusters that do not contain boron (MCI = 0.074–0.077); whereas mixed $B_2Al_4^{2-}$, $Al_2B_4^{2-}$, and $Ga_2B_4^{2-}$ D_{4h} clusters containing boron atoms are less aromatic (MCI = 0.032–0.047). For planar structures, there are basically two groups of clusters. First, the group formed by B_6^{2-} and $B_2Al_4^{2-}$ has eight valence electrons distributed in two π-MOs and two σ-MOs (*vide infra*). Therefore, having four π-electrons and four σ-electrons, they are σ- and π-antiaromatic species. Second, the group formed by Al_6^{2-}, Ga_6^{2-}, $Al_2B_4^{2-}$, $Al_2Ga_4^{2-}$, $Ga_2B_4^{2-}$, and $Ga_2B_4^{2-}$ have eight valence electrons distributed in one π-MO and three σ-MOs (*vide infra*) and, therefore, they are σ- and π-aromatic species.

With the aim to obtain a deeper insight into the origin of 2D to 3D relative energies an energy decomposition analysis was performed, following the reaction presented in Scheme 1. As pointed out above, both systems can be constructed from two identical X_3^- anionic fragments, both in their quintet state in order to form the corresponding new bonds. Three of these bonds are of σ character, two tangential (σ^T) and one radial (σ^R), and one π character (see Fig. 2). It must be pointed out that, very recently, Mercero *et al.* have proven the multiconfigurational character of some of the lowest-lying electronic states of Al_3^-.[19] In the case of the quintet state of Al_3^-, which is the fragment used in our calculations, the authors showed that the electronic configuration of the four valence electrons is also derived from the occupation of two σ-type tangential and one σ-type radial molecular orbitals arising from the $3p_x$ and $3p_y$ atomic orbitals, and one π-type orbital arising from the $3p_z$ ones. This quintet state was found to be dominated by one-single configuration with a coefficient of 0.92 in the multiconfigurational wavefunction.[19] Moreover, the energy difference between the ground state and the quintet state was almost the same when computed at DFT or at the MCSCF levels of theory.[19] This seems to indicate that DFT methods give reasonable results for this quintet state. Finally, the T_1 test[64] applied to clusters collected in Table 1 was found to be always less than 0.045, thus indicating the relatively low multiconfigurational character of these species. It is commonly accepted that CCSD(T) produces acceptable results for T_1 values as high as 0.055.[65]

The different terms of the EDA for B_6^{2-}, Al_6^{2-}, and Ga_6^{2-} clusters are enclosed in Table 2. First we notice that the total bonding energies (ΔE) are much larger for B_6^{2-} than for Al_6^{2-} or Ga_6^{2-}. For the former, ΔE are −100.2 (O_h) and −179.5 kcal mol^{-1} (D_{2h}), whereas for the two latter are in between −19.0 and −38.1 kcal mol^{-1}. This trend correlates with the shorter B–B bond lengths mentioned above. Table 2 also encloses the relative EDA energies between the two clusters. The B_3^- fragment taken from the B_6^{2-} system in its D_{2h} symmetry is the one that suffers the largest deformation, *i.e.* the largest change in geometry with respect to the fully relaxed B_3^- cluster in the quintet state (ΔE_{dist} = 12.5 kcal mol^{-1}), whereas the rest of the systems present small values of ΔE_{dist} (0.0–1.7 kcal mol^{-1}). However, differences in ΔE are not due to distortion energies (indeed ΔE_{dist} values follow the opposite trend as ΔE), but to interaction energies (ΔE_{int}).

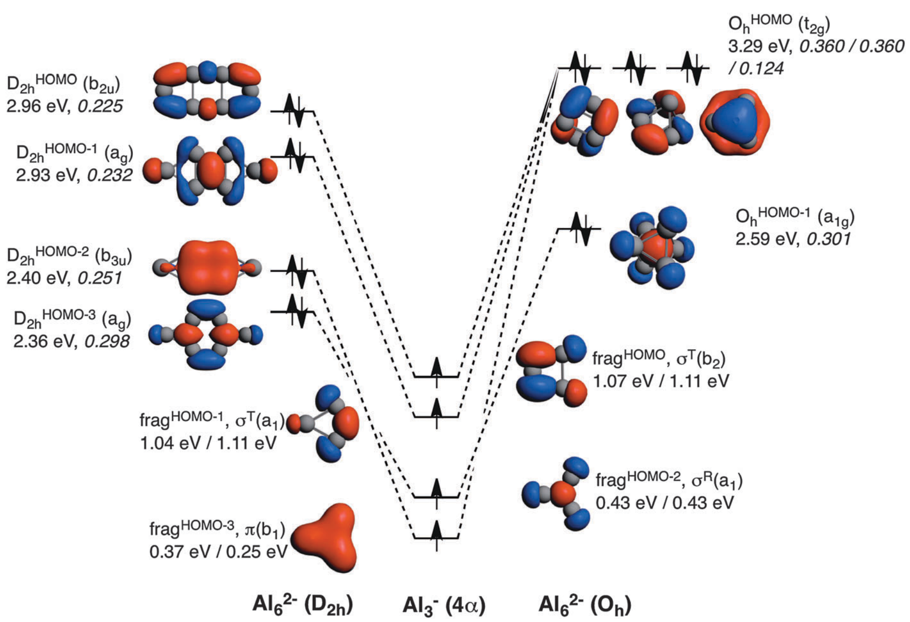

Fig. 2 Molecular orbital diagram corresponding to the formation of Al_6^{2-} in D_{2h} and O_h symmetries from two Al_3^- fragments in their quintet state. Energies of the molecular orbitals are enclosed (in eV), as well as the ⟨SOMO|SOMO⟩ overlaps of the fragments (values in italics). Energies of the fragments obtained from both D_{2h} (left) and O_h (right) symmetries are also enclosed.

Table 2 Energy decomposition analysis (EDA) of X_6^{2-} (X = B, Al, and Ga) metal clusters with D_{2h} and O_h symmetries (in kcal mol^{-1}), from two X_3^- fragments in their quintet state, computed at the BLYP-D3(BJ)/TZ2P level

	B_6^{2-}			Al_6^{2-}			Ga_6^{2-}		
	$D_{2h} + D_{2h} \to D_{2h}$	$O_h + O_h \to O_h$	$\Delta(\Delta E)$	$D_{2h} + D_{2h} \to D_{2h}$	$O_h + O_h \to O_h$	$\Delta(\Delta E)$	$D_{2h} + D_{2h} \to D_{2h}$	$O_h + O_h \to O_h$	$\Delta(\Delta E)$
ΔE_{int}	−192.0	−101.4	*−90.6*	−20.7	−39.8	*19.1*	−19.1	−31.0	*11.9*
ΔE_{Pauli}	533.5	735.3	*−201.8*	225.7	348.0	*−122.3*	269.6	384.5	*−114.9*
ΔV_{elstat}	−239.0	−291.9	*52.9*	−96.3	−166.5	*70.2*	−138.0	−207.5	*69.5*
ΔE_{oi}	−483.4	−542.8	*59.4*	−146.9	−217.4	*70.5*	−146.7	−203.4	*56.7*
ΔE_{disp}	−3.2	−2.1	*−1.1*	−3.2	−3.9	*0.7*	−4.0	−4.7	*0.6*
ΔE_{dist}	12.5	1.3	*11.2*	0.0	1.7	*−1.7*	0.1	1.4	*−1.3*
ΔE	−179.5	−100.2	*−79.3*	−20.7	−38.1	*17.4*	−19.0	−29.6	*10.6*

Thus, we focus on the decomposition of ΔE_{int} into ΔE_{Pauli}, ΔV_{elstat}, ΔE_{oi}, and ΔE_{disp} terms. As a general trend, in all three X_6^{2-} clusters ΔE_{Pauli} is larger for the O_h than the D_{2h} cluster ($\Delta(\Delta E_{Pauli})$ = −201.8, −122.3, and −114.9 kcal mol^{-1} for B_6^{2-}, Al_6^{2-}, and Ga_6^{2-}, respectively), so making it less stable. The overlaps between doubly occupied MOs are larger in the more compact O_h structure that, consequently, has larger ΔE_{Pauli}. The larger difference in ΔE_{Pauli} between the O_h and D_{2h} structures in the case of B_6^{2-} as compared to Al_6^{2-} and Ga_6^{2-} is attributed to the particularly short B–B distances that increase the overlap between doubly occupied MOs of each B_3^- fragment. At the same time, the O_h form presents larger (more negative) electrostatic interactions ($\Delta(\Delta V_{elstat})$ = 52.9, 70.2, and 69.5 kcal mol^{-1} for B_6^{2-}, Al_6^{2-}, and Ga_6^{2-}, respectively). It is usually the case that higher destabilising Pauli repulsions go with larger stabilising electrostatic interactions. The reason has to be found in the fact that both interactions increase in the absolute value when electrons and nuclei are confined in a relatively small space. The electrostatic interaction together with orbital interaction ($\Delta(\Delta E_{oi})$ = 59.4, 70.5, and 56.7 kcal mol^{-1} for B_6^{2-}, Al_6^{2-}, and Ga_6^{2-}, respectively) terms favour the O_h structure. However, in the case of O_h B_6^{2-}, $\Delta(\Delta V_{elstat})$ and $\Delta(\Delta E_{oi})$ cannot compensate $\Delta(\Delta E_{Pauli})$, which causes the D_{2h} system to be the lowest in energy. The opposite occurs for Al_6^{2-} and Ga_6^{2-}. Finally, the dispersion term almost does not affect the relative energies, as the difference in dispersion is only in the order of *ca.* 1.0 kcal mol^{-1}. Therefore, what causes the different trend observed for B_6^{2-} on one side, and Al_6^{2-} and Ga_6^{2-} on the other side is basically the ΔE_{oi} term, which combined with the ΔV_{elstat} component does (Al_6^{2-} and Ga_6^{2-}) or does not (B_6^{2-}) compensate the higher ΔE_{Pauli} of the O_h form.

The comparison of the MOs diagrams of B_6^{2-} and Al_6^{2-}, built from their X_3^- fragments, justify the trends of ΔE_{oi} (see Fig. 2 and 3). Both D_{2h} and O_h clusters are built from the same fragments; the only difference is that the two tangential $\text{frag}^{\text{HOMO}}(\sigma^T(b_2))$ and $\text{frag}^{\text{HOMO}-1}(\sigma^T(a_1))$ MOs of Al_3^- are degenerate when obtained from Al_6^{2-} in its O_h geometry, whereas they are not when generated from the D_{2h} system, although they still are very close in energy. As discussed from the EDA, O_h is more stable than D_{2h} because of more stabilizing electrostatic and orbital interactions, which compensate its larger Pauli repulsion. Fig. 2 also encloses the overlaps for the interactions between the four SOMOs of the Al_3^- fragments to form the MOs of the metal clusters in both geometries. We take the Al_3^- fragments in their quintet states with three unpaired σ- and one unpaired π-electrons, all of them with spin α in one fragment and β in the other. A more negative ΔE_{oi} in O_h Al_6^{2-} is justified from the larger ⟨SOMO|SOMO⟩ overlaps, especially for t_{2g} O_h^{HOMOa} and O_h^{HOMOb} (0.360 compared to 0.225 and 0.232 for b_{2u} D_{2h}^{HOMO} and a_g $D_{2h}^{\text{HOMO}-1}$, respectively). D_{2h} only presents a larger overlap for the π fragment orbital (0.251 for b_{3u} $D_{2h}^{\text{HOMO}-2}$ and 0.124 for t_{2g} O_h^{HOMOc}). Meanwhile both of them have almost the same overlap for the combination of the radial MO (σ^R) fragment ($\text{frag}^{\text{HOMO}-2}$), with ⟨SOMO|SOMO⟩ = 0.298 and 0.301 for a_g $D_{2h}^{\text{HOMO}-3}$ and $O_h^{\text{HOMO}-1}$, respectively. Overall, the higher orbital interaction term of the O_h system can be explained by the larger ⟨SOMO|SOMO⟩ overlaps of two of the t_{2g} delocalised molecular orbitals for this cluster (see Fig. 2). The energies of the occupied MOs of Al_6^{2-} formed are higher than those of the Al_3^- SOMOs because we move from a monoanionic fragment to a dianionic molecule.

Now it is the turn to visualize the MOs of B_6^{2-}. The fragments for B_3^- are the same as those for Al_3^- (see Fig. 3). However, the first difference appears in the MOs for B_6^{2-} with D_{2h} symmetry. In this case, it would be more reasonable to build the MOs of this molecule from two triplet (not quintet) B_3^- fragments. The reason is the different occupation of the MOs when compared to the D_{2h} Al_6^{2-} species. In D_{2h} B_6^{2-}, the HOMO corresponds to the antibonding π MO. To reach doubly occupied bonding (b_{3u} $D_{2h}^{\text{HOMO}-4}$) and antibonding (b_{2g} D_{2h}^{HOMO}) π MOs, the π MO ($\text{frag}^{\text{HOMO}-3}$) should be doubly occupied. Furthermore, the tangential $\sigma^T(a_1)$ $\text{frag}^{\text{HOMO}}$ does not participate in any occupied MO of this metal cluster and only generates virtual MOs. Consequently, MOs of B_6^{2-} are better formed from two B_3^- fragments in their triplet state (see red electron in Fig. 3). On the other hand, B_6^{2-} with O_h follows the same trend as Al_6^{2-}, and in this case the same SOMOs in their quintet state are involved. At this point, it is worth mentioning that, as pointed out by Mercero *et al.*, due to the strong multiconfigurational character of this species, one must be cautious with the electronic configuration, especially for the triplet state, as radial and tangential MOs are very close in energy.[19]

To make results comparable, Table 2 gathers the EDA of O_h and D_{2h} B_6^{2-} from two B_3^- fragments in their quintet states. Also in this case ΔE_{oi} is more favourable for O_h than for D_{2h}, however, at a lower extent when compared to Al_6^{2-}. There are two main reasons for such a decrease of the strength of ΔE_{oi} in O_h compared to D_{2h}. First, and more importantly, because

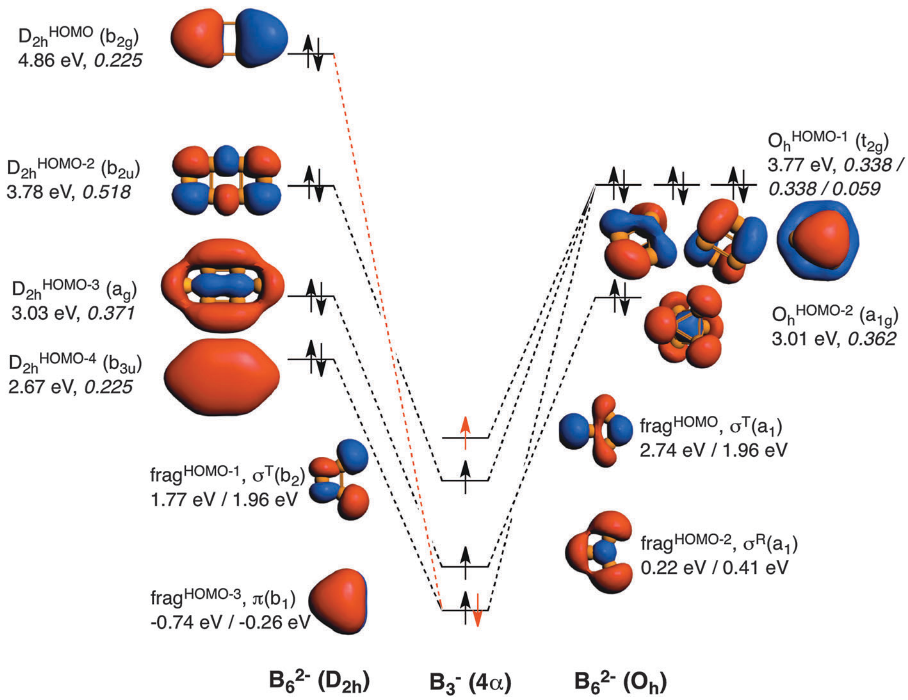

Fig. 3 Molecular orbital diagram corresponding to the formation of B_6^{2-} in D_{2h} and O_h symmetries from two B_3^- fragments in their quintet states. Electrons in red refer to the formation of B_6^{2-} (D_{2h}) from B_3^- fragments in their triplet state. In the triplet state, $\pi(b_1)$ is doubly occupied, σ^R(a1) and $\sigma^T(b_2)$ remain singly occupied, and the $\sigma^T(a_1)$ becomes unoccupied. Energies of the molecular orbitals are enclosed (in eV), as well as the ⟨SOMO|SOMO⟩ overlaps of the fragments (values in italics). Energies of the fragments obtained from both D_{2h} (left) and O_h (right) symmetries are also enclosed.

the D_{2h}^{HOMO-2} formed presents a much larger ⟨SOMO|SOMO⟩ overlap than t_{2g} O_h^{HOMO-1} (0.518 in the former *vs.* 0.338 in the latter). In particular, this D_{2h}^{HOMO-2} MO contributes to the 2c–2e B–B localised bonds that are related to the larger covalent character of this structure. And second, because the π-interaction between the two π SOMO fragments is much larger in the case of D_{2h} (0.225 *vs.* 0.059 for D_{2h} and O_h, respectively). Nevertheless, these two more favourable orbital interactions are not enough to surpass the ΔE_{oi} term of the O_h cluster. However, as compared to Al_6^{2-}, for B_6^{2-} the $\Delta(\Delta E_{oi})$ term favours the O_h system to a less extent and cannot compensate the higher ΔE_{Pauli} term of the O_h form, thus making the planar geometry to be more stable in this case. This is related to the determinant force of the formed covalent bonding, involving more localised MOs than for Al_6^{2-}. Such a larger covalent component in B_6^{2-} is also supported by the covalent character of the interaction between the two fragments calculated as % covalency = $(\Delta E_{oi}/(\Delta E_{oi} + \Delta V_{elstat} + \Delta E_{disp})) \times 100$. This formula results in B_6^{2-}: 65–67% (O_h, D_{2h}), Al_6^{2-}: 56–60% (O_h, D_{2h}), and Ga_6^{2-}: 49–51% (O_h, D_{2h}); thus confirming again the larger covalency found in B_6^{2-}.

Finally, as done usually in the turn-upside-down approach,[36–39,56,66,67] instead of building X_6^{2-} in O_h symmetry from the corresponding two X_3^- fragments obtained from the O_h structure, we can build the O_h system from two X_3^- fragments extracted from the X_6^{2-} cluster in D_{2h} symmetry, and viceversa (see Tables S2–S4 in the ESI‡). The main conclusions remain unaltered and confirm that the D_{2h} structures suffer a lower Pauli repulsion whereas those of O_h symmetry have more favourable electrostatic and orbital interactions. The interplay between the Pauli repulsion on the one hand and electrostatic and orbital interactions on the other determines the most favorable symmetry in each case.

Just to conclude this section, we must point out that the whole EDA and turn-upside-down analyses were performed with fragments in their quintet state. However, as we commented before this is not the most reasonable way to build B_6^{2-} in D_{2h} symmetry. Table S5 (ESI‡) contains the EDA for O_h and D_{2h} B_6^{2-} systems using B_3^- fragments in their triplet states. Results show that although the different terms are larger in the absolute value, the trends discussed above are not affected, and the D_{2h} cluster is favoured mainly because of smaller Pauli repulsions.

Mixed metal clusters

In this section, we analyse the $X_2Y_4^{2-}$ clusters with X, Y = B, Al, Ga and X ≠ Y (see Fig. 4). The relative energies of the planar and 3D forms are also enclosed in Table 1. In all cases, the D_{2h} system is preferred when the cluster incorporates four B atoms; otherwise the 3D D_{4h} geometry is the lowest in energy. In particular, the D_{2h} symmetry is much more stable for $Al_2B_4^{2-}$ and $Ga_2B_4^{2-}$ by 66.9 and 79.4 kcal mol^{-1}, respectively. On the other hand, when B is not the predominant atom, the D_{4h} cluster is more stable by about 9–16 kcal mol^{-1}. As for the homoatomic metal clusters, at the CCSD(T) level, the same trend is obtained, although the D_{4h} system is stabilized with respect to the D_{2h} one by 20–30 kcal mol^{-1}. It is important to note that the D_{4h} and D_{2h} systems are not always the most stable for the $X_2Y_4^{2-}$ clusters. For instance, for $Al_2B_4^{2-}$, a C_2 geometry is the most stable form and, for $B_2Al_4^{2-}$, a C_{2v} structure is the

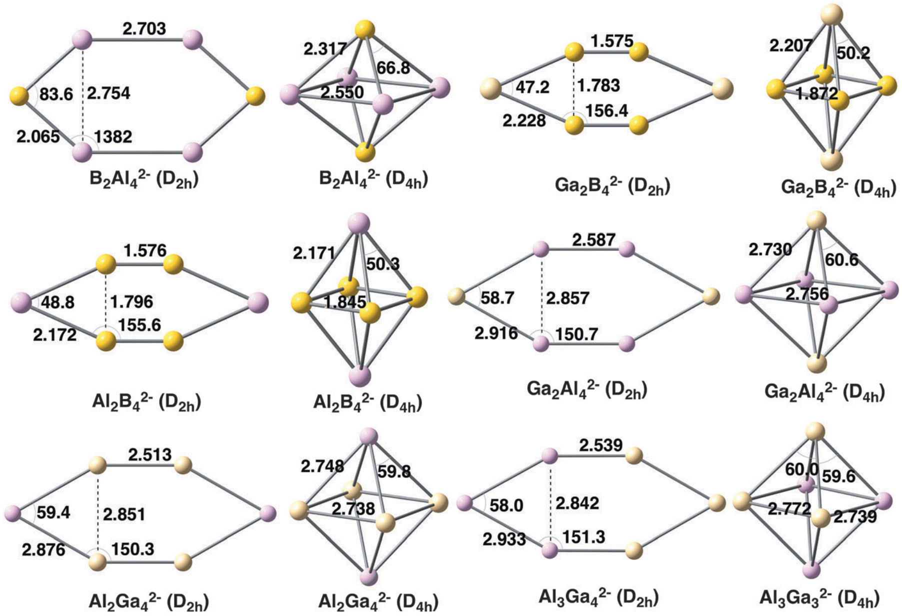

Fig. 4 Geometries of mixed metal clusters analysed with planar and 3D geometries. Distances in Å and angles in degrees.

lowest in energy.[18] However, we are not interested here in finding the most stable structure for each cluster but to discuss the reasons why in some cases 2D clusters are preferred over 3D and the other way round. Finally, $Al_3Ga_3^{2-}$ also prefers an O_h geometry by 13.2 kcal mol^{-1}. Unfortunately, this latter relative energy cannot be compared to those of $B_3Al_3^{2-}$ or $B_3Ga_3^{2-}$ because the strength of the localised bonding between three B atoms prevents the optimization of their 3D structures. In this context, it is worth mentioning that Alexandrova and coworkers[26] found in X_3Y_3 (X = B, Al, Ga; Y = P, As) clusters that the lighter elements prefer 2D structures, whereas the heavier ones favour 3D geometries.

The EDA was also performed for this series of six mixed metal clusters (see Table 3) with the aim to further understand the determinant force towards the most stable cluster. For the $X_2Y_4^{2-}$ clusters, the EDA was carried out taken YXY^- fragments in their quintet states. For $Al_3Ga_3^{2-}$, the fragments were Al_3^- and Ga_3^- in the quintet state too. For those systems for which the out-of-plane geometry is the most stable, the combination of more favourable electrostatic and orbital interactions, even though presenting larger Pauli repulsion, gives the explanation to the trend observed. This is the same behaviour already discussed above for both Al_6^{2-} and Ga_6^{2-} systems. On the other hand, when D_{2h} symmetry is the cluster lower in energy, as for $Al_2B_4^{2-}$ and $Ga_2B_4^{2-}$ metal clusters, even though the D_{4h} system presents more stable electrostatic interaction, now the orbital interactions in combination with less unfavourable Pauli repulsion favour the D_{2h} symmetry. This latter behaviour differs from that of B_6^{2-}, for which the orbital interactions also favour the O_h symmetry, thus making Pauli repulsion the determinant factor towards the preference for planar D_{2h} B_6^{2-}.

Table 3 Energy decomposition analysis (EDA) of all mixed metal clusters with planar and 3D symmetries (in kcal mol^{-1}), from two fragments at their quintet states, computed at the BLYP-D3(BJ)/TZ2P level

		ΔE_{int}	ΔE_{Pauli}	ΔV_{elstat}	ΔE_{oi}	ΔE_{disp}
$B_2Al_4^{2-}$	D_{4h}	−52.1	440.1	−202.7	−285.7	−3.9
	D_{2h}	−40.4	243.4	−98.1	−182.5	−3.3
	ΔE	11.7	−196.7	104.6	103.2	0.6
$Al_2B_4^{2-}$	D_{4h}	−75.1	584.0	−251.7	−404.1	−3.3
	D_{2h}	−139.6	556.6	−238.6	−454.5	−3.3
	ΔE	−64.6	−27.4	13.2	−50.4	0.0
$Al_2Ga_4^{2-}$	D_{4h}	−35.0	381.2	−201.0	−210.6	−4.6
	D_{2h}	−19.2	283.1	−147.1	−151.4	−3.8
	ΔE	15.8	−98.1	53.8	59.3	0.8
$Ga_2B_4^{2-}$	D_{4h}	−83.8	590.4	−262.5	−408.2	−3.5
	D_{2h}	−157.5	540.0	−225.6	−468.6	−3.2
	ΔE	−73.7	−50.4	36.8	−60.4	0.3
$Ga_2Al_4^{2-}$	D_{4h}	−38.4	370.1	−188.0	−216.1	−4.3
	D_{2h}	−20.6	218.0	−90.8	−144.4	−3.6
	ΔE	17.8	−152.0	97.3	71.7	0.8
$Al_3Ga_3^{2-}$	D_{3h}	−36.8	381.0	−197.8	−215.7	−4.2
	C_{3v}	−20.7	254.4	−122.8	−148.7	−3.6
	ΔE	16.1	−126.6	75.0	67.0	0.6

Conclusions

In previous studies,[18] the preference of B_6^{2-} for the planar D_{2h} geometry and of Al_6^{2-} for the 3D O_h one was justified by the inclination for localised covalent bonding in the former cluster and delocalised bonding in the latter. These two effects point in opposite directions. In the present work, we go one-step further by showing that the preference of B_6^{2-} for the planar D_{2h} form is due to two particular molecular orbital interactions. From one side the $D_{2h}^{HOMO-1}(b_{2u})$ formed from two tangential SOMO $\sigma^T(b_2)$ orbitals. This orbital is related to localised covalent bonding, and has a much more important weight in B_6^{2-} than in Al_6^{2-}, proving the dominant localised covalent character in the former. And the second determinant interaction is that of π character. In the case of $O_h^{HOMO-1}(t_{2g})$ for B_6^{2-}, its formation from two π SOMO orbitals is much less favourable than for Al_6^{2-}. This result is in line with a dominant delocalisation force in Al clusters and more localised bonding in B metal clusters. For mixed clusters, we have found that those with more than two B atoms prefer the planar structure for same reasons discussed for B_6^{2-}.

Acknowledgements

This work was supported by the Ministerio de Economía y Competitividad (MINECO) of Spain (Project CTQ2014-54306-P) and the Generalitat de Catalunya (project 2014SGR931, Xarxa de Referència en Química Teòrica i Computacional, ICREA Academia 2014 prize for M.S., and grant No. 2014FI_B 00429 to O. E. B.). The EU under the FEDER grant UNGI10-4E-801 (European Fund for Regional Development) has also funded this research. J. P. thanks the National Research School Combination-Catalysis (NRSC-C), and The Netherlands Organization for Scientific Research (NWO/CW and NWO/NCF). The authors are grateful to Dr Ferran Feixas for fruitful discussions.

References

1 Y. Hu, T. J. Wagener, Y. Gao, H. M. Meyer and J. H. Weaver, *Phys. Rev. B: Condens. Matter Mater. Phys.*, 1988, **38**, 3037–3044.
2 B. Wang, H. Wang, H. Li, C. Zeng, J. G. Hou and X. Xiao, *Phys. Rev. B: Condens. Matter Mater. Phys.*, 2000, **63**, 035403.
3 V. Torma, T. Reuter, O. Vidoni, M. Schumann, C. Radehaus and G. Schmid, *ChemPhysChem*, 2001, **2**, 546–548.
4 R. N. Barnett, C. L. Cleveland, H. Häkkinen, W. D. Luedtke, C. Yannouleas and U. Landman, *Eur. Phys. J. D*, 1999, **9**, 95–104.
5 S. Aldridge and A. J. Downs, *The Group 13 Metals Aluminium, Gallium, Indium and Thallium: Chemical Patterns and Peculiarities*, John Wiley & Sons, Ltd, Chichester, 2011.
6 A. N. Alexandrova, K. A. Birch and A. I. Boldyrev, *J. Am. Chem. Soc.*, 2003, **125**, 10786–10787.
7 A. N. Alexandrova and A. I. Boldyrev, *Inorg. Chem.*, 2004, **43**, 3588–3592.
8 A. N. Alexandrova, A. I. Boldyrev, H.-J. Zhai and L.-S. Wang, *Coord. Chem. Rev.*, 2006, **250**, 2811–2866.
9 H.-J. Zhai, A. N. Alexandrova, L.-S. Wang and A. I. Boldyrev, *Angew. Chem., Int. Ed.*, 2003, **42**, 6004–6008.
10 A. I. Boldyrev and L.-S. Wang, *Chem. Rev.*, 2005, **105**, 3716–3757.
11 A. E. Kuznetsov, K. A. Birch, A. I. Boldyrev, X. Li, H.-J. Zhai and L.-S. Wang, *Science*, 2003, **300**, 622–625.
12 A. E. Kuznetsov, A. I. Boldyrev, H.-J. Zhai, X. Li and L.-S. Wang, *J. Am. Chem. Soc.*, 2002, **124**, 11791–11801.
13 X. Li, A. E. Kuznetsov, H.-F. Zhang, A. Boldyrev and L.-S. Wang, *Science*, 2001, **291**, 859–861.
14 A. E. Kuznetsov, A. I. Boldyrev, H.-J. Zhai, X. Li and L.-S. Wang, *J. Am. Chem. Soc.*, 2002, **124**, 11791–11801.
15 O. C. Thomas, W.-J. Zheng, T. P. Lippa, S.-J. Xu, S. A. Lyapustina and K. H. Bowen, *J. Chem. Phys.*, 2001, **114**, 9895–9900.
16 A. N. Alexandrova, A. I. Boldyrev, H.-J. Zhai and L.-S. Wang, *J. Chem. Phys.*, 2005, **122**, 054313.
17 A. N. Alexandrova, A. I. Boldyrev, H.-J. Zhai, L.-S. Wang, E. Steiner and P. W. Fowler, *J. Phys. Chem. A*, 2003, **107**, 1359–1369.
18 M. T. Huynh and A. N. Alexandrova, *J. Phys. Chem. Lett.*, 2011, **2**, 2046–2051.
19 J. M. Mercero, E. Matito, F. Ruipérez, I. Infante, X. Lopez and J. M. Ugalde, *Chem. – Eur. J.*, 2015, **21**, 9610–9614.
20 C. Corminboeuf, C. S. Wannere, D. Roy, R. B. King and P. v. R. Schleyer, *Inorg. Chem.*, 2006, **45**, 214–219.
21 O. El Bakouri, M. Duran, J. Poater, F. Feixas and M. Solà, *Phys. Chem. Chem. Phys.*, 2016, DOI: 10.1039/c5cp07011b.
22 J. Ma, Z. Li, K. Fan and M. Zhou, *Chem. Phys. Lett.*, 2003, **372**, 708–716.
23 L.-M. Yang, J. Wang, Y.-H. Ding and C.-C. Sun, *Phys. Chem. Chem. Phys.*, 2008, **10**, 2316–2320.
24 A. N. Alexandrova, *Chem. Phys. Lett.*, 2012, **533**, 1–5.
25 A. N. Alexandrova, M. J. Nayhouse, M. T. Huynh, J. L. Kuo, A. V. Melkonian, G. Chavez, N. M. Hernando, M. D. Kowal and C.-P. Liu, *Phys. Chem. Chem. Phys.*, 2012, **14**, 14815–14821.
26 A. N. Alexandrova, M. R. Nechay, B. R. Lydon, D. P. Buchan, A. J. Yeh, M.-H. Tai, I. P. Kostrikin and L. Gabrielyan, *Chem. Phys. Lett.*, 2013, **588**, 37–42.
27 J. E. Fowler and J. M. Ugalde, *J. Phys. Chem. A*, 2000, **104**, 397–403.
28 J. E. Fowler and J. M. Ugalde, *Phys. Rev. A: At., Mol., Opt. Phys.*, 1998, **58**, 383–388.
29 P. Farràs, N. Vankova, L. L. Zeonjuk, J. Warneke, T. Dülcks, T. Heine, C. Viñas, F. Teixidor and D. Gabel, *Chem. – Eur. J.*, 2012, **18**, 13208–13212.
30 M. R. Fagiani, L. Liu Zeonjuk, T. K. Esser, D. Gabel, T. Heine, K. R. Asmis and J. Warneke, *Chem. Phys. Lett.*, 2015, **625**, 48–52.
31 J. K. Olson and A. I. Boldyrev, *J. Phys. Chem. A*, 2013, **117**, 1614–1620.
32 K. Kitaura and K. Morokuma, *Int. J. Quantum Chem.*, 1976, **10**, 325–340.
33 K. Morokuma, *Acc. Chem. Res.*, 1977, **10**, 294–300.
34 T. Ziegler and A. Rauk, *Theor. Chim. Acta*, 1977, **46**, 1–10.
35 T. Ziegler and A. Rauk, *Inorg. Chem.*, 1979, **18**, 1558–1565.
36 M. El-Hamdi, W. Tiznado, J. Poater and M. Solà, *J. Org. Chem.*, 2011, **76**, 8913–8921.
37 M. El-Hamdi, O. El Bakouri El Farri, P. Salvador, B. A. Abdelouahid, M. S. El Begrani, J. Poater and M. Solà, *Organometallics*, 2013, **32**, 4892–4903.
38 M. El-Hamdi, M. Solà, G. Frenking and J. Poater, *J. Phys. Chem. A*, 2013, **117**, 8026–8034.
39 R. Islas, J. Poater, E. Matito and M. Solà, *Phys. Chem. Chem. Phys.*, 2012, **14**, 14850–14859.
40 G. te Velde, F. M. Bickelhaupt, E. J. Baerends, C. Fonseca Guerra, S. J. A. van Gisbergen, J. G. Snijders and T. Ziegler, *J. Comput. Chem.*, 2001, **22**, 931–967.
41 A. D. Becke, *Phys. Rev. A: At., Mol., Opt. Phys.*, 1988, **38**, 3098–3100.

42 C. Lee, W. Yang and R. G. Parr, *Phys. Rev. B: Condens. Matter Mater. Phys.*, 1988, **37**, 785–789.
43 S. Grimme, J. Antony, S. Ehrlich and H. Krieg, *J. Chem. Phys.*, 2010, **132**, 154104.
44 S. Grimme, S. Ehrlich and L. Goerigk, *J. Comput. Chem.*, 2011, **32**, 1456–1465.
45 M. J. Frisch, G. W. Trucks, H. B. Schlegel, G. E. Scuseria, M. A. Robb, J. R. Cheeseman, G. Scalmani, V. Barone, B. Mennucci, G. A. Petersson, H. Nakatsuji, M. Caricato, X. Li, H. P. Hratchian, A. F. Izmaylov, J. Bloino, G. Zheng, J. L. Sonnenberg, M. Hada, M. Ehara, K. Toyota, R. Fukuda, J. Hasegawa, M. Ishida, T. Nakajima, Y. Honda, O. Kitao, H. Nakai, T. Vreven, J. A. Montgomery Jr., J. E. Peralta, F. Ogliaro, M. Bearpark, J. J. Heyd, E. Brothers, K. N. Kudin, V. N. Staroverov, R. Kobayashi, J. Normand, K. Raghavachari, A. Rendell, J. C. Burant, S. S. Iyengar, J. Tomasi, M. Cossi, N. Rega, J. M. Millam, M. Klene, J. E. Knox, J. B. Cross, V. Bakken, C. Adamo, J. Jaramillo, R. Gomperts, R. E. Stratmann, O. Yazyev, A. J. Austin, R. Cammi, C. Pomelli, J. W. Ochterski, R. L. Martin, K. Morokuma, V. G. Zakrzewski, G. A. Voth, P. Salvador, J. J. Dannenberg, S. Dapprich, A. D. Daniels, Ö. Farkas, J. B. Foresman, J. V. Ortiz, J. Cioslowski and D. J. Fox, *Gaussian 09, Revision A.02 ed.*, Gaussian, Inc., Pittsburgh, PA, 2009.
46 J. Cizek, *J. Chem. Phys.*, 1966, **45**, 4256–4266.
47 G. D. Purvis III and R. J. Bartlett, *J. Chem. Phys.*, 1982, **76**, 1910–1918.
48 K. Raghavachari, G. W. Trucks, J. A. Pople and M. Head-Gordon, *Chem. Phys. Lett.*, 1989, **157**, 479–483.
49 T. H. Dunning Jr., *J. Chem. Phys.*, 1989, **90**, 1007–1023.
50 R. A. Kendall, T. H. Dunning Jr. and R. J. Harrison, *J. Chem. Phys.*, 1992, **96**, 6796–6806.
51 F. M. Bickelhaupt and E. J. Baerends, in *Rev. Comput. Chem.*, ed. K. B. Lipkowitz and D. B. Boyd, Wiley-VCH, New York, 2000, vol. 15, pp. 1–86.
52 F. M. Bickelhaupt, A. Diefenbach, S. P. de Visser, L. J. de Koning and N. M. M. Nibbering, *J. Phys. Chem. A*, 1998, **102**, 9549–9553.
53 C. Fonseca Guerra, J.-W. Handgraaf, E. J. Baerends and F. M. Bickelhaupt, *J. Comput. Chem.*, 2004, **25**, 189–210.
54 I. Fernández and G. Frenking, *Faraday Discuss.*, 2007, **135**, 403–421.
55 I. Fernández and G. Frenking, *Chem. – Eur. J.*, 2007, **13**, 5873–5884.
56 R. Islas, J. Poater and M. Solà, *Organometallics*, 2014, **33**, 1762–1773.
57 F. Feixas, E. Matito, J. Poater and M. Solà, *Wiley Interdiscip. Rev.: Comput. Mol. Sci.*, 2013, **3**, 105–122.
58 P. Bultinck, R. Ponec and S. Van Damme, *J. Phys. Org. Chem.*, 2005, **18**, 706–718.
59 F. Feixas, E. Matito, J. Poater and M. Solà, *Chem. Soc. Rev.*, 2015, **44**, 6434–6451.
60 J. Poater, M. Duran, M. Solà and B. Silvi, *Chem. Rev.*, 2005, **105**, 3911–3947.
61 E. Matito, M. Duran and M. Solà, *J. Chem. Phys.*, 2005, **122**, 014109.
62 E. Matito, *ESI-3D: Electron Sharing Indexes Program for 3D Molecular Space Partitioning*, Institute of Computational Chemistry and Catalysis, Girona, 2006, http://iqc.udg.es/~eduard/ESI.
63 S. Alvarez, *Dalton Trans.*, 2013, **42**, 8617–8636.
64 T. J. Lee and P. R. Taylor, *Int. J. Quantum Chem., Quantum Chem. Symp.*, 1989, **S23**, 199–207.
65 J. M. L. Martin, in *Energetics of Stable Molecules and Reactive Intermediates*, ed. M. S. Minas da Piedade, Kluwer Academic Publishers, Dordrecht, 1999, vol. 535, pp. 373–417.
66 J. Poater, R. Visser, M. Solà and F. M. Bickelhaupt, *J. Org. Chem.*, 2007, **72**, 1134–1142.
67 E. Díaz-Cervantes, J. Poater, J. Robles, M. Swart and M. Solà, *J. Phys. Chem. A*, 2013, **117**, 10462–10469.